Original Article

Film cooling optimization on leading edge gas turbine blade using differential evolution

Juan C García[1], José O Dávalos[2], Gustavo Urquiza[1],
Sergio Galván[3], Alberto Ochoa[2], José A Rodríguez[1] and
Carlos Ponce[2]

Abstract

This article reports the optimization of film cooling on a leading edge of a gas turbine blade model, with showerhead configuration, it is based on five input parameters, which are hole diameter, hole pitch, column holes pitch, injection angle, and velocity at plenum inlet. This optimization increased the Area-Averaged Film Cooling Effectiveness (η_{Aav}) and reduced the consumption of coolant flow. Differential Evolution assisted by artificial neural networks was used as optimization algorithm. Reynolds Averaged Navier–Stokes computations were carried out to getting the net database and to evaluate the optimized models predicted by artificial neural network. The results show an effective increment of η_{Aav} by 36% and a mass flow reduction by 66%. These results were reached by means of a better distribution of cooling flow at blade surface as function of the input parameters. To assure the reliability of the numerical model, particle image velocimetry technique was used for its validation.

Introduction

Higher inlet temperatures are required to increase the gas turbine power. However, this has a negative impact on the turbine blades integrity, mainly in the zone of the leading edge, which presents the most exposition to the thermal loads. The film cooling is a technique used to prevent damages on blades by thermal loads. In this technique, air taken from compressor is ejected through small holes placed on the blade surface in order to avoid the contact between the blade itself and the hot mainstream. The main handicap of film cooling is the reduction of the gas turbine output power because the usage of compressed air. Then, the aim of an optimal film cooling design is to get a good cooling performance with the minimum amount of coolant air. The film cooling performance is highly influenced by the flow characteristics and geometric parameters of the cooling holes such as diameter and injection angle.[1] Experimental and numerical investigations have been carried out to study separately the effects of the mentioned parameters.[2–6] Nevertheless, the study of parameters interacting simultaneously to obtain a cooling optimum design is a complicated task and for this reason new

computational tools are needed. Recently, optimization methods have been implemented to obtain objective and efficient evaluations of the performance of industrial flows. Part of this research has been focused on design shape optimization (DSO) of turbomachinery components like film-cooled blades.

Evolutionary algorithms (EA) are optimization methods based on the biological evolution and they have proved to be reliable in the optimization of nonlinear process. EA are widely used in the optimization of turbomachinery components.[7–11] Verstraete et al.[12] presented a study about the design of internal cooling

[1]Instituto de Investigación en Ciencias Básicas y Aplicadas, Universidad Autónoma del Estado de Morelos, Morelos, México
[2]Instituto de Ingeniería y Tecnología, Universidad Autónoma de Ciudad Juárez, Chihuahua, México
[3]Facultad de Ingeniería Mecánica, Universidad Michoacana de San Nicolás de Hidalgo, Michoacán, México

Corresponding author:
José O Dávalos, Instituto de Ingeniería y Tecnología, Universidad Autónoma de Ciudad Juárez, Av. Del Charro 450, Col. Partido Díaz, Ciudad Juárez, Chihuahua 32310, México.
Email: jose.davalos@uacj.mx

channels of a gas turbine blade. The objective of their research was to increase the blade lifetime reducing the cooling mass flow consumption using genetic algorithms (GA) as optimization method. The input variables were diameter of channels and its spatial positions. Their results showed that the use of EA, like GA, in the optimization procedure, increased the blade lifetime limiting the cooling flow. A study about the film cooling optimization of a turbine vane pressure side was carried out by Johnson et al.[13] They used GA based on the geometrical parameters of cooling holes. Their results showed a reduction of average near-wall gas temperature of 2 K and a reduction of maximum heat flux of 2 kW/m^2. Verstraete and Li[14] realized the multi-objective optimization on a U-bend in a serpentine internal cooling channels using Differential Evolution (DE). Lee et al.[15] performed the optimization of a row of film cooling holes by means of a Hybrid Multi-Objective Evolutionary Algorithm. They defined two objectives functions, one for increasing film cooling effectiveness and another for reducing the aerodynamic losses. As surrogated method, they used a Response Surface Approximation. Nowak and Wróblewsky[16] optimized the cooling system of a turbine guide vane using GA. They compared a Binary GA against Continuous GA. They concluded that significant improvements of the temperature reduction on the blade surface are observed with the Continuous GA. Chi et al.[17] perform a geometrical optimization of non-uniform impingement cooling structure varying diameter jet holes using GA. They found that the improvement of overall cooling performance mainly relied on the temperature reduction at pin-fin array. A more uniform temperature is obtained with a non-uniform pin-fin array. El Ayoubi et al.[18] carried out an aerothermal shape optimization of a double row of film cooling holes on the suction side of a turbine vane. Results showed that the optimization decreased the aerodynamic losses and at the same time increased cooling effectiveness.

The aim of this work is to increase the Area-Averaged Film Cooling Effectiveness η_{Aav} on a leading edge of a gas turbine blade model with a minimum amount of coolant mass flow, using optimization techniques combined with Reynolds Average Navier–Stokes (RANS) computations. DE optimization technique was employed as an algorithm to find the optimal case. The input parameters were diameter and angle of cooling holes, pitch between holes, pitch between row of holes, and velocity of coolant at plenum inlet. Objective function was evaluated by means of artificial neural networks (ANN) trained with a database based on a two levels full factorial design of experiments. Optimal specimens (OS) from DE are evaluated with three-dimensional RANS computations; results are compared with ANN predictions and stored in the existing database to start a new analysis until it performs 20 DE runs.

RANS computations were validated in a low speed tunnel with particle image velocimetry (PIV) measurements. The final results have given evidence that for an adequate η_{Aav}, a reduction of coolant mass flow was made possible by an optimization using DE assisted with surrogated techniques like ANN and RANS.

Methodology

Optimization strategy

Tools based on RANS, optimization algorithms and ANN have been introduced to evaluate the performance of hydraulic structures and machinery, and these provide a valuable complement to traditional engineering methods. Parts of those tools have been focused on optimizing the shape of turbomachinery components.

In case of film cooling gas turbine blade, any optimization method requires a large data set, which in some cases could be obtained by a large number of RANS computations. A large data set is necessary to evaluate many different cases before reaching an OS satisfying objective function. Although this procedure allows to have the possibility of finding an efficient film cooling area, it is expensive in terms of computational time due to the evaluation of the individual's fitness, which is the most time-consuming component of the optimization. To highlight the advantages of this methodology, Figure 1 presents a flowchart with the steps proposed in order to find the best η_{Aav}, reducing the coolant flow. In the first step, different specimens with defined configurations of the input
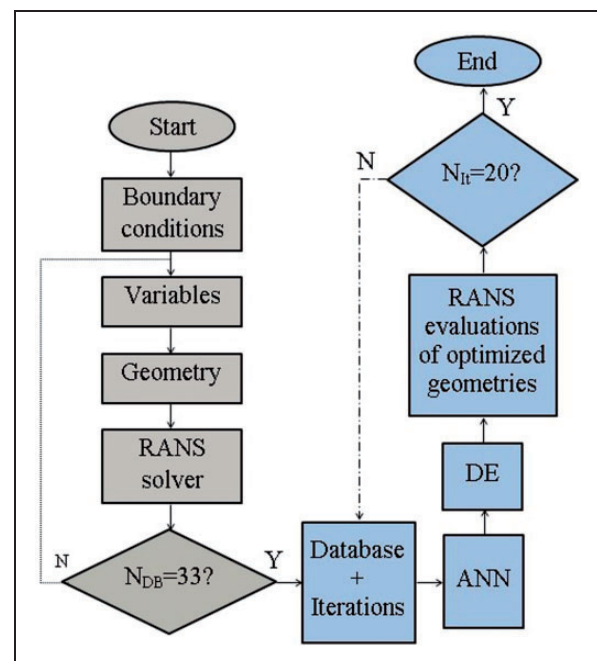

Figure 1. Optimization methodology.

parameters were established through a two-level full factorial design of experiments. Every single specimen configuration was stated using geometrical and flow parameters. Four geometrical parameters (hole diameter, ejection angle, column pitch, and hole pitch) and one flow parameter (velocity) were considered. A set of 33 specimens (NDB = 33) were generated according with the design of experiment and then they were evaluated using RANS computations. In this way, it was gotten a complete database for the 33 combinations of variables (specimens) and its respective η_{Aav} computations and cooling flow were obtained. RANS computations were validated using PIV measurements in an additional specimen.

As next step, the ANN was trained using the data set obtained by RANS computations and an ANN model to predict the cooling effectiveness and cooling flow was generated. This model was used for the DE algorithm to evaluate the objective function and to obtain the design variables for the optimal film cooling performance. The objective function was evaluated quickly by the ANN, but due to the database size, this prediction could be wrong and a final verification of the optimized variables for the best film cooling performance is needed by means of the RANS solver. These results are added to a database to increase its size and the prediction capability of ANN. This procedure was repeated through 20 iterations (It = 20).

Objective function definition

To find an optimum case using an EA, it is necessary to state an objective function, as follows

$$F_{obj}(V) = w_\eta F(\eta_{Aav}) + w_{\dot{m}} F(\dot{m}) \tag{1}$$

This is a mathematical function, which in the case of gas turbine film cooling, should find the best Area-Averaged Film Cooling Effectiveness (η_{Aav}), while the consumption of coolant flow ($\dot{m}$) is decreased. In the case of cooling gas turbine blades, the coolant flow should be decreased because affect total power and efficiency of gas turbine cycle.

$F_{obj}(V)$ contains the five input parameters defined as design variables. The first term of the right $F(\eta_{Aav})$ is the η_{Aav} objective, which has a weight of $w_\eta = 0.7$, which declares its importance in the equation. The η_{Aav} objective is the difference between a defined cooling effectiveness target and the cooling effectiveness calculated in function of the vector of variables. The effectiveness target η_{tar} was set to 1, this means that the value of the difference could never be less than zero

$$F(\eta_{Aav}) = \eta_{tar} - \eta_{Aav}(V) \tag{2}$$

The second term of equation (1), $F(\dot{m})$, represents the cooling flow objective and it has a weight of $w_{\dot{m}} = 0.3$, which establishes the importance of $F(\dot{m})$

and is computed with equation (3) during the optimization process

$$F(\dot{m}) = \frac{\dot{m}(V) - \dot{m}_{tar}}{\dot{m}_{tar}} \tag{3}$$

where $\dot{m}(V)$ is the cooling mass flow, whereas the mass flow target $\dot{m}_{tar}$ was set to 1×10^{-5} kg/s.

The η_{Aav} is defined by equation (4)

$$\eta_{Aav} = \frac{1}{A} \iint \eta \, dA \tag{4}$$

where A is the film cooling area and η is the adiabatic effectiveness, which is defined by

$$\eta = \frac{T_m - T_{aw}}{T_m - T_c} \tag{5}$$

here T_{aw} is the adiabatic temperature, T_m is the mainstream temperature, and T_c is the coolant temperature at the exit of cooling hole.

At plenum inlet, the amount of coolant mass flow is defined by

$$\dot{m} = nM\rho_m v_m A_c \tag{6}$$

where n is the number of cooling holes, $M = \frac{\rho_c v_c}{\rho_m v_m}$ is a given blowing ratio, ρ and v are density and velocity of mainstream, respectively, and A_c is the area of cooling holes.

DE optimization method

DE is an evolutionary optimization method developed by Storn and Price.[19] The main objective of DE is to find an individual that minimizes a defined objective function. This method proceeds through three genetic operators: mutation, recombination, and selection. In this way, a population is randomly generated in which each individual is represented by a vector. These vectors consist mostly out of input parameters that define every case of study. From this population, a vector is selected, $X_t^g = (X_1, X_2, X_3, \ldots X_n)$, where g is the number of generation and t is the number of vector. Three additional vectors p_t^g, q_t^g, r_t^g, are chosen, so that they are different to X_t^g. A new trial vector is generated in the mutation process, which is defined by

$$Y_{t,i}^g = p_{t,i}^g + F\left(q_{t,i}^g + r_{t,i}^g\right) \quad i = 1 \ldots n \tag{7}$$

where n is the vector length and $F \in [0, 1]$ is a scale factor. In the recombination process, a vector Z_t^{g+1} is obtained using X_t^g and Y_t^g. This process is defined by

$$Z_{t,i}^{g+1} = \begin{cases} Y_{t,i}^g & r_i < C \\ X_{t,i}^g & r_i \geqslant C \end{cases} \tag{8}$$

where r_i is a random number between 0 and 1 and C is a crossover rate parameter. Finally, the resulting new vector $\mathbf{Z}_t^{g+1}$ will replace the vector $\mathbf{X}_t^g$, in a new generation, only if its fitness values have been improved, otherwise the vector $\mathbf{X}_t^g$ will pass to the next generation without changes. This procedure is repeated until the population of the new generation is completed.

For the optimization of η_{Aav} in this work, DE was applied through 300 generations with a population of 50 specimens. The scale factor and the crossover rate parameter were set to 0.4 and 0.8, respectively.

ANN

ANN was used as method to evaluate the objective function replacing the RANS solver. ANN is an interpolator tool that can be used to solve a variety of tasks like classification, regression, estimation problems, etc. The net is formed by layers composed of neurons: one input layer, one or more hidden layers, and one output layer. Each layer is linked with the subsequent layer by means of weighted connections. Between input and hidden layer, a weighted sum of inputs and a bias are made; the result of this sum is used as argument for the transfer function to obtain the output of the hidden layer

$$O_{out} = g[\omega_{out}f(\omega_{in}in_k + b_{1s}) + b_{2l}] \quad (9)$$

where f and g are the transfer functions for hidden and output layer, respectively, ω_o is the weight of output layer, in are the net inputs, b_1 and b_2 are the bias of hidden layer and output layer, respectively;

$k, s,$ and l are the number of neurons in input layer, hidden layer, and output layer, respectively. In this work, hyperbolic tangent sigmoid (equation (10)) and linear (equation (11)) were the transfer functions for the hidden and the output layer, respectively

$$f = \frac{2}{1 + e^{[2*(\omega_{in}*in_k + b_{1s})]}} - 1 \quad (10)$$

$$g = \omega_{out} * f + b_{2l} \quad (11)$$

Two ANN models were constructed, first to predict the η_{Aav} and second to predict the mass flow consumption. The database was divided into training and validation sets each of one contains 80% and 20%, respectively, of database size. Both models contain three layers with five neurons in the input layer, four neurons in the hidden layer, and one neuron in the output layer. The number of neurons in the hidden layer was selected based on the ANN performance that was evaluated by the root mean square error (RMSE; Figure 2(a)). The net architecture for η_{Aav} predictions is shown in Figure 2(b). The adjustment of weights and biases was made using the Levenberg–Marquardt training algorithm, one of the training algorithms recommended for networks of moderate size.[20] Comparison of η_{Aav} predicted with ANN versus η_{Aav} predicted with RANS during training and validation is presented in Figure 3(a). In addition, in Figure 3(b), five new RANS simulations were performed to test the ANN obtaining a RMSE = 0.0102. These results assure a good correlation between ANN and RANS.
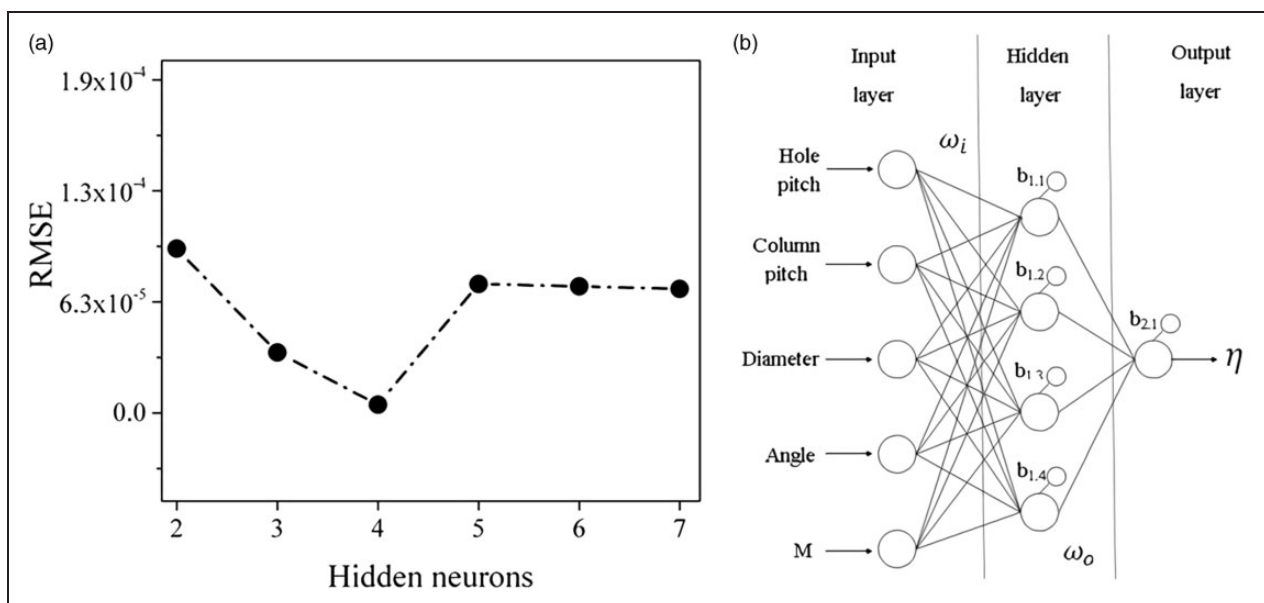

Figure 2. Construction of ANN: (a) Selection of hidden neurons based in RMSE and (b) ANN architecture.
ANN: artificial neural networks; RMSE: root mean square error.

Description of experimental rig

RANS computations were used in the generation of database and in the comparison of the optimized models obtained with surrogated methods. To validate RANS computations, experimental measurements were carried out in a low speed wind tunnel with a test section with dimensions of $0.5 \times 0.5 \times 0.25$ m^3. Using the PIV technique, flow field was measured in zones around the leading edge. The configuration of the experimental array is presented in Figure 4(a). Air from the exterior is suctioned by an axial fan and it is delivered to wind tunnel with a velocity of 10 m/s. In a seeding box, tracer particles generated by a fog
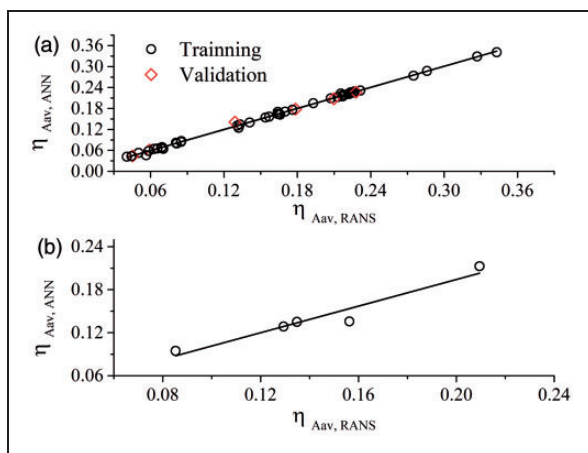

Figure 3. RANS and ANN comparison during (a) training and validation, and (b) five new tests.
ANN: artificial neural networks; RANS: Reynolds Average Navier–Stokes.

machine are seeded in the air from a compressor. The flow seeded is distributed into the plenum chamber and into the wind tunnel, where it is mixed with the mainstream flow. To control velocity and temperature at plenum inlet, a hot wire probe was placed at this location. The leading edge specimen (Figure 4(b)) represents the leading edge of a gas turbine blade, and it consists of a semi-circular body and flat after body. The model has one row of five cooling holes at stagnation line and two rows of four cooling holes at each side of the stagnation line. The rows are separated 30° between them. Diameter of cooling holes is 2 mm. The supply plenum is cylindrical and it has a diameter of 12.70 mm and a length of 95 mm. Pitch between holes is 10 mm. The semi-circular chord has a length c equal to 125 mm.

The PIV equipment used in this work was a laser Nd:YAG with double cavity laser. Dimensions of the target area and the interrogation area were 105×80 mm^2 and 64×64 pixels, respectively. Interval time between laser pulses was 3.3 μs with an error estimation of less than 5%. The sampling frequency was 10 Hz. Images were acquired with a CCD camera, which has a spatial resolution of 128×102.4 mm^2. Distance between camera and zone of interest was about 1 m. Laser and camera were synchronized by a Dantec System Hub. Fog particles of 1–5 microns of diameter were seeded in the flow by a fog generator inside a Plexiglas box.

RANS model

RANS computations were carried out to generate initial database population and later to verify the computed η_{Aav} using ANN surrogate model of the best
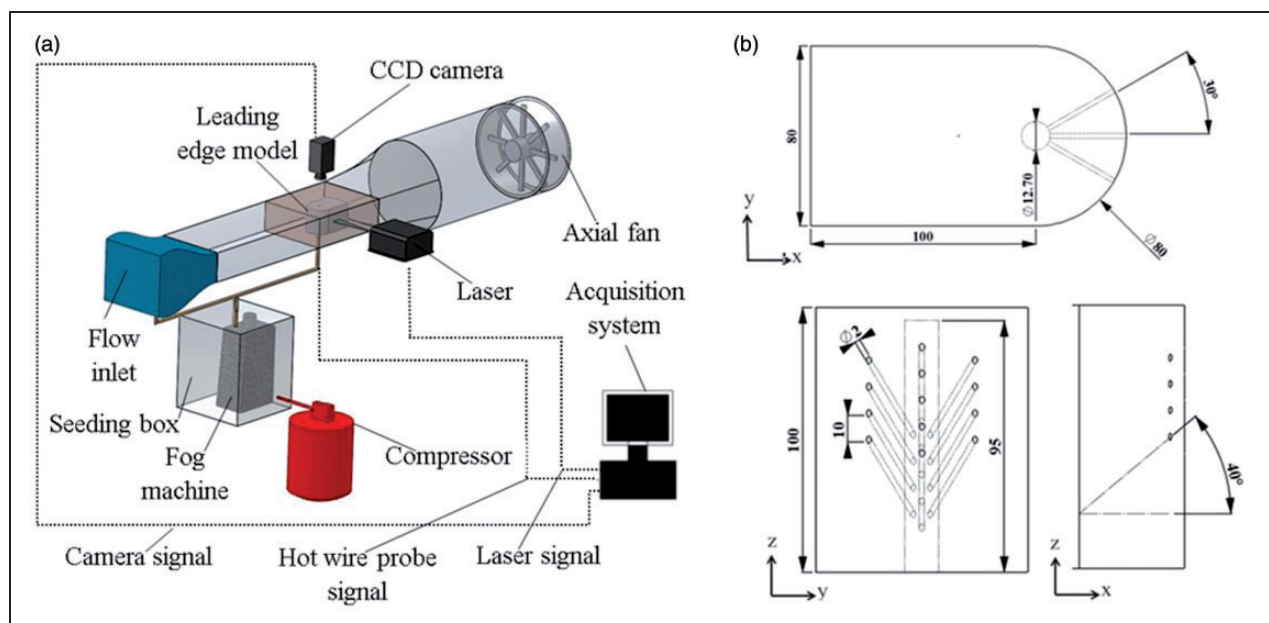

Figure 4. Schematic representation of the experimental setup (a) and detailed view of the leading edge model (b).

specimens proposed by DE Optimization algorithm. The numerical domain, of the test section, consists of three zones: mainstream flow, plenum flow, and a solid zone that represents the leading edge model. Velocity inlet was set as boundary condition at mainstream inlet and at plenum inlet, whereas pressure outlet condition was used for the domain outlet. The boundary condition for leading edge wall was adiabatic and a no-slip condition was considered. Both domains and boundary conditions are presented in Figure 5.

RNG $\kappa - \epsilon$ model was used to solve the turbulence during RANS computations.[21] For the spatial discretization, the second-order up-wind scheme was employed, whereas pressure and velocity were coupled by means of SIMPLEC algorithm. For continuity, momentum and turbulence, the convergence criterion

was set at 1×10^{-5} and, for the energy equation, it was 1×10^{-8}. For this analysis, a structured mesh with hexahedral elements was used. Two views of the meshed computational domain are shown in Figure 6(a). The mesh size was defined based on an independence grid study, where the temperature profile between two cooling holes on blade wall was monitored. For the independence grid study, four meshes were used (Figure 6(b)). The difference between the temperature profiles computed with the meshes of 3,532,144 and 4,290,868 cells was 0.28%. For this reason and with the purpose of reducing the computational cost, the mesh selected for this research was the mesh with 3,532,144 elements with $0.1 < y+ < 1$.

Generation of database

To create database, using the validated RANS model, 33 additional simulations were performed based on a full factorial two levels DOE. In order to accelerate the optimization process, a Matlab code was generated to create the geometry of specimens, to mesh the domain and to launch the RANS solver. The lower and upper ranges of input parameters for these simulations are listed in Table 1.
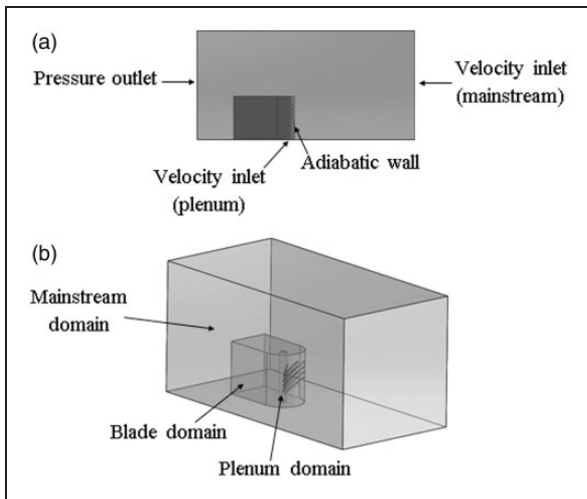

Figure 5. Location of (a) boundary conditions and (b) computational domains.

Table 1. Levels of the input parameters.

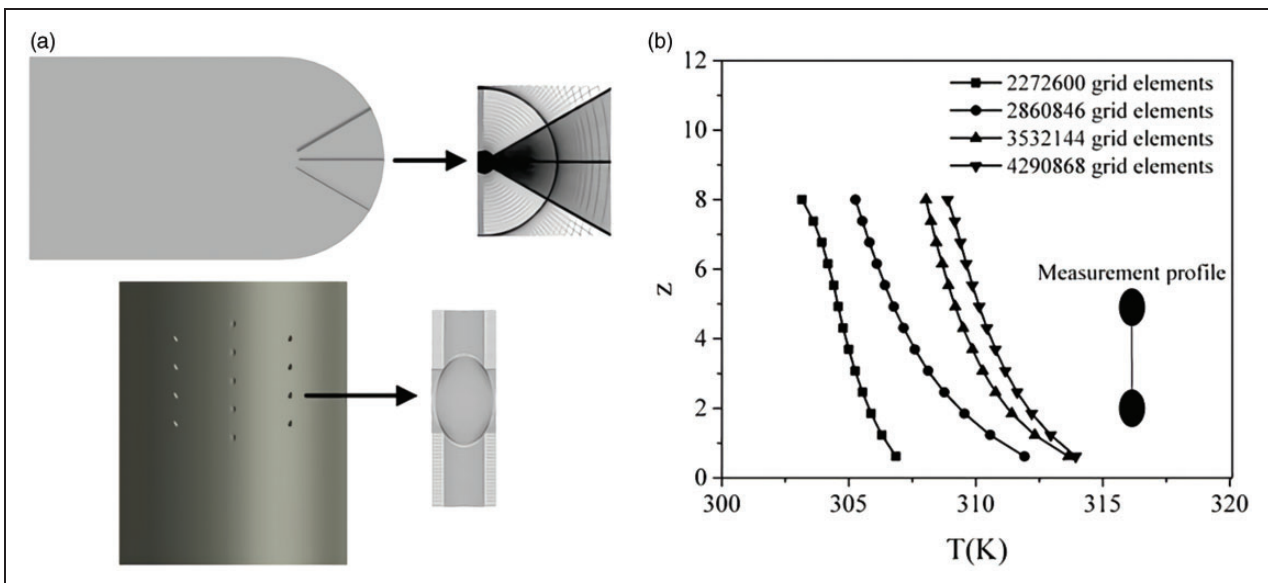| Parameter	Upper	Lower
Hole pitch (mm)	3	9
Column pitch (mm)	3	6
Diameter (mm)	0.6	1.3
Angle (°)	25	35
Velocity (m/s)	0.175	1.5

Figure 6. Details of discretized model: (a) mesh and (b) independence grid study.

The lower and upper range of velocity magnitudes correspond to blowing ratios of M = 0.5 and M = 2, respectively. In DOE, the parameters can assume two values, low and high, that belong to the 25% and 75% of the range. The number of specimens was defined by 2^n, where 2 represents two levels and n is the quantity of parameters involved. For this research, the number of specimens was 32 plus an additional specimen with all the parameters with average values. In all cases, the temperature ratio Tc/Tm was equal to 0.5.
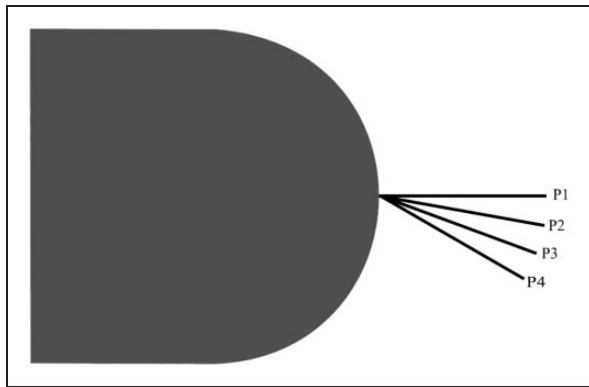

Figure 7. Location of profiles used to compare RANS and PIV results.
RANS: Reynolds Average Navier–Stokes; PIV: particle image velocimetry.

Results

Validation

The experimental and numerical results were compared at four profiles (P1, P2, P3, P4) separated 5° between them, these profiles were located at the vicinity of leading edge (Figure 7). The profiles are extended following the stagnation line, from the exit middle hole of first row to mainstream. Each profile has a length l = 4 cm. The comparison was carried out under a blowing ratio of M = 0.5.

Results of velocity profiles comparison are presented in Figure 8. In order to dimensionless the profiles, its length (l) were divided by the cooling hole diameter D. It is observed that there is a good match between the RANS and the experimental results. Discrepancies appears downstream from the film cooling zone (l/D < 5) due to fluctuations of the incoming air and to the PIV spatial discretization, which is too large and cannot be to capture data near the blade surface, but the overall prediction presents a good agreement. An error about 10% between measured and predicted profiles was calculated by means of mean square error.

The validation of temperature was presented by Dávalos et al.[22] for the same model and using the same RANS methodology. Thermocouples were placed over surface blade to monitoring the distribution of the temperature. Results showed a prediction error about 3% at stagnation line of cooling holes and about 6% at lateral cooling holes.
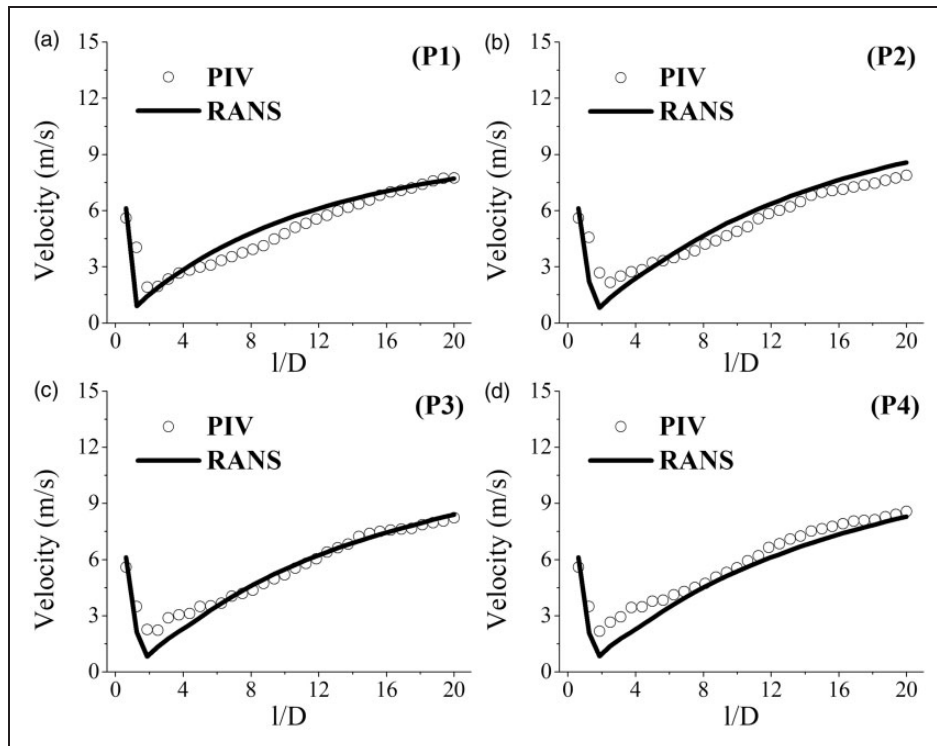

Figure 8. Comparison of RANS and PIV velocity profiles P1, P2, P3, and P4.
RANS: Reynolds Average Navier–Stokes; PIV: particle image velocimetry.

Optimization results

DE was used as optimization method to improve the η_{Aav} on a gas turbine blade model with a minimal amount of coolant mass flow. The ANN surrogate method acted as the evaluator of objective function. The optimization was carried out through 20 iterations in which the objective function for the new specimens was evaluated using the ANN and such evaluation was compared with RANS calculations and the
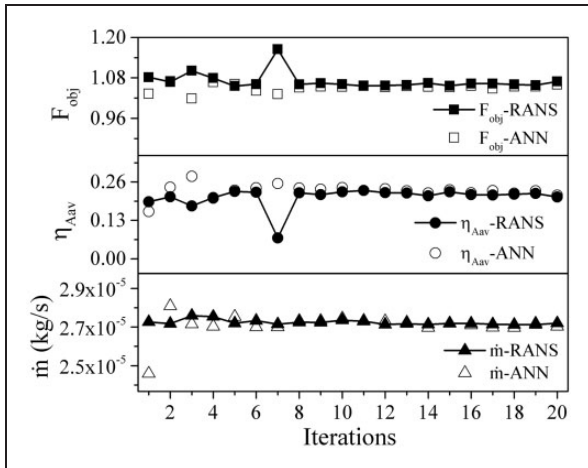
optimized specimen was added to database to increase its accuracy.

The objective function, Area-Averaged Film Cooling Effectiveness (η_{Aav}) and cooling mass flow were computed by RANS and ANN, during the DE optimization process (Figure 9). In the first iterations, the results predicted with ANN did not match correctly with the RANS results; however, after the iteration 8, the ANN learning was improved due to enrichment of database and a good prediction of the objective function was obtained. After this point, minimal changes were observed in the value of objective function remaining between 1.05 and 1.06.

Figure 10 shows the values of F_{obj}, η_{Aav}, and $F(\dot{m})$ for the initial database specimens (NDB), for the specimens (DE) found trough the DE optimization and for the OS found during the optimization process. The values of η_{Aav} and $F(\dot{m})$ were improved considerably by DE. Some of the first 33 specimens had a better η_{Aav} than the optimized ones, however their consumption of mass flow were higher.

The values of the objective function, η_{Aav} and mass flow consumption of the OS are presented in Table 2. The best specimen of the initial set of 33, referred now as ODB, was added to Table 2 to compare the changes occurred through the optimization process. The OS had an objective function 60% lower than in the case of ODB. In addition, the η_{Aav} increased 36.41%, whereas mass flow was reduced around 65%.

Figure 9. Objective function $\left(F_{obj}\right)$, Area-Averaged Film Cooling Effectiveness (η_{Aav}), and cooling mass flow ($\dot{m}$) computed by RANS and ANN during the optimization process. RANS: Reynolds Average Navier–Stokes; ANN: artificial neural networks.
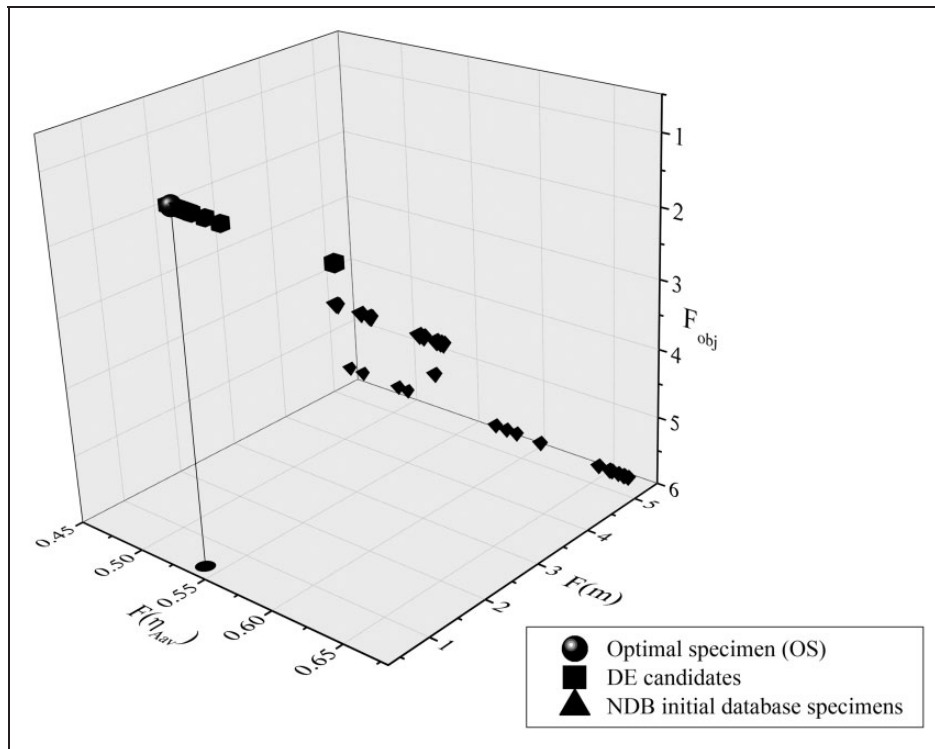

Figure 10. Comparison of optimized specimens vs. initial database specimens.

The input variables values of the optimized specimen and the specimen from initial database are shown in Table 3. The results indicate that values of both hole pitch and column pitch are near to their lowest range, this means that an improvement in η_{Aav} can be gotten reducing the distance between holes and hole columns at leading edge. On the other hand, the hole diameter was close to upper range. Because of the magnitude of injection angle did not show a defined trend, it can be assumed that this parameter had a small influence in film cooling. The velocity at plenum inlet took values close to its lowest range; this corresponds to a reduction of mass flow consumption owing to the relationship between them.

In Figure 11, contours of film cooling effectiveness for the OS and ODB are presented. There is a remarkable difference between the hole diameters size and its location. Another change is the reduction of pitch hole, which also causes that the area between holes diminishes. For the OS, the cooling flow discharge covers better the blade surface than the ODB specimen because of the smaller area. Comparing both film cooling effectiveness contours, it is observed the reduction of zones with poor coverage for the OS, like in the space between holes of the lateral columns. The reduction of these hot points diminishes the risk of high thermal gradients and consequently the thermal stresses could be also reduced. The direction of wakes of the film cooling jets differs as consequence of changes in the geometry of the OS; in the model without optimization the jet is deflected to the spanwise direction, whereas in the improved one, the jet follows the streamwise direction.

Figure 12 depicts the film cooling effectiveness profiles at the first hole of the lateral column and at middle hole of the stagnation line column. In both graphs downstream of hole, film cooling was considerably improved due to a better coverage of cooling flow at leading edge. It is at the lateral column where the difference between the OS and the ODB specimen is higher.
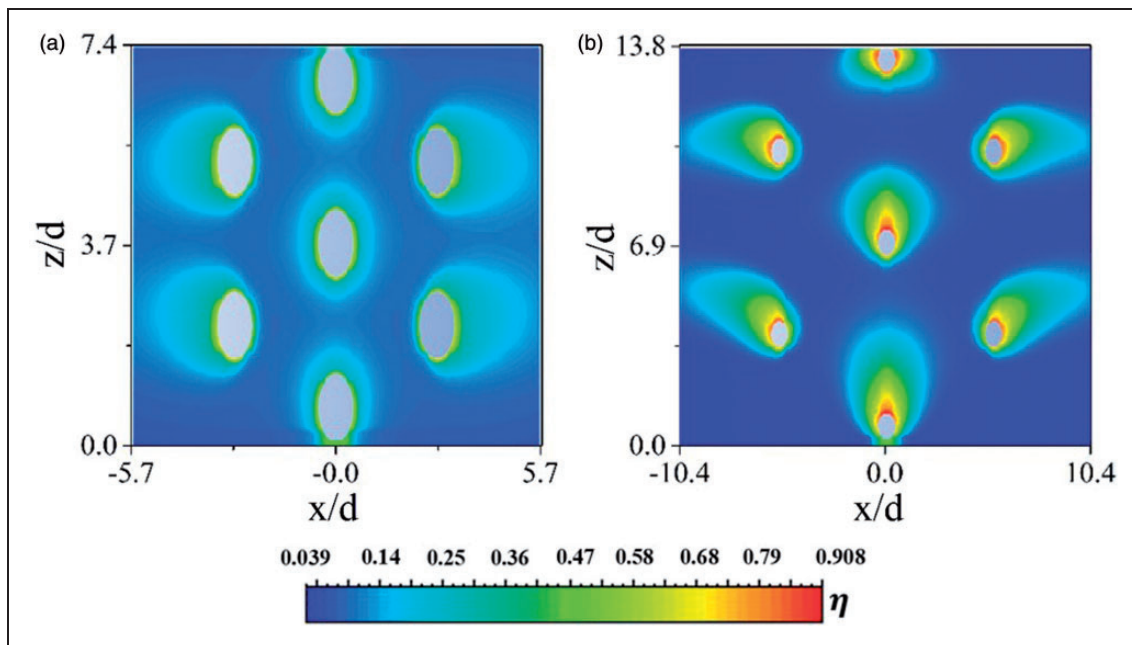
Table 2. Objective function, η_{Aav}, and mass flow of OS vs. ODB.

	F_{obj}	η_{Aav}	$\dot{m}$
ODB	2.6399	0.1697	7.839×10^{-5}
OS	1.0559	0.2315	2.726×10^{-5}

ODB: best specimen of the initial database; OS: optimal specimen.

Table 3. Geometrical characteristics for OS and ODB.

	OS	ODB
Hole pitch (mm)	3.007	4.5
Column pitch (mm)	3.517	3.75
Diameter (mm)	1.275	0.7
Injection angle (°)	35.468	33
Velocity (m/s)	0.175	0.506

ODB: best specimen of the initial database; OS: optimal specimen.

Figure 11. Comparison of film cooling effectiveness at leading edge between OS (a) and ODB (b).
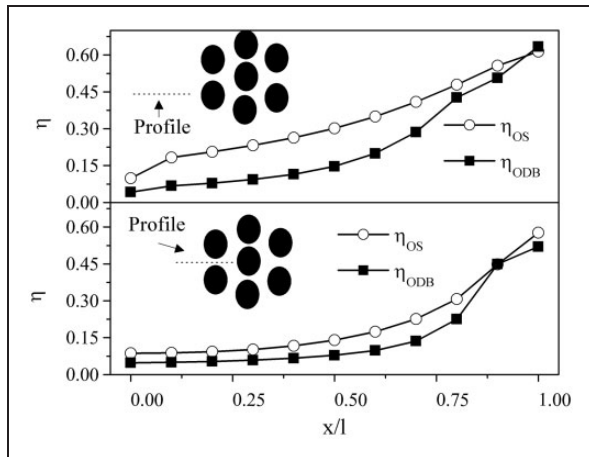OS: optimal specimen; ODB: best specimen of the initial database.

Figure 12. Cooling effectiveness profiles at lateral column and stagnation line.

Conclusions

In this research, a DE optimization algorithm was applied to improve the Area-Averaged Film Cooling Effectiveness with a minimum amount of coolant air from compressor. In addition to DE, the optimization methodology included ANN and the RANS computations. The ANN was used as surrogated method to evaluate the fitness that allows to reduce the computational costs of the RANS computations. The OS had an increase of the cooling effectiveness about 36% and a mass flow reduction about 65% with respect to the ODB. The geometrical characteristics of the OS showed that reducing the area between holes, by means of short hole pitch and short column pitch, the cooling of leading edge is increased. Also, a big diameter film cooling hole presented a better distribution of coolant, reducing zones without good film cooling and providing a more uniform temperature avoiding thermal gradients in leading edge surface. Thus, this method optimized the cooling effectiveness and could be used in the design of film cooling of gas turbine blades.

References

1. Bogard DG and Thole KA. Gas turbine film cooling. *J Propul Power* 2006; 22: 249–270.
2. Sangan CM, Zhou K, Litherland K, et al. Thermal imaging as flow visualization for gas turbine film cooling. *Proc IMechE, Part G: J Aerospace Engineering* 2011; 225: 417–431.
3. Gräf L and Kleiser L. Large-eddy simulation of double-row compound-angle film cooling: Setup and validation. *Comput Fluids* 2011; 43: 58–67.
4. Asghar FH and Hyder MJ. Computational study of film cooling from single and two staggered rows of novel semi-circular cooling holes including coolant plenum. *Energy Convers Manage* 2011; 52: 329–334.
5. Dyson TE, Bogard DG, Piggush JD, et al. Overall effectiveness for a film cooled turbine blade leading edge with varying hole pitch. *J Turbomach* 2013; 135: 0310111–0310118.
6. Ling J, Coletti F, Yapa SD, et al. Experimentally informed optimization of turbulent diffusivity for a discrete hole film cooling geometry. *Int J Heat Fluid Flow* 2013; 44: 348–357.
7. Mengistu T and Ghaly W. Aerodynamic optimization of turbomachinery blades using evolutionary methods and ANN-based surrogate models. *Optim Eng* 2007; 9: 239–255.
8. Bonaiuti D and Zangeneh M. On the coupling of inverse design and optimization techniques for the multiobjective, multipoint design of turbomachinery blades. *J Turbomach* 2009; 131: 0210141–02101416.
9. Song L, Luo C, Li J, et al. Aerodynamic optimization of axial turbomachinery blades using parallel adaptive range differential evolution and Reynolds-averaged Navier-Stokes solutions. *Int J Numer Meth Biomed Eng* 2011; 27: 283–303.
10. Asgarshamsi A, Benisi AH, Assempour A, et al. Multi-objective optimization of lean and sweep angles for stator and rotor blades of an axial turbine. *Proc IMechE, Part G: J Aerospace Engineering* 2014; 229: 906–916.
11. Joly MM, Verstraete T and Paniagua G. Integrated multifidelity, multidisciplinary evolutionary design optimization of counterrotating compressors. *Integr Comput-Aid Eng* 2014; 21: 249–261.
12. Verstraete T, Amaral S, Van den Braembussche R, et al. Design and optimization of the internal cooling channels of a high pressure turbine blade—Part II: Optimization. *J Turbomach* 2010; 132: 0210141–02101419.
13. Johnson JJ, King PI, Clark JP, et al. Genetic algorithm optimization of a high-pressure turbine vane pressure side film cooling array. *J Turbomach* 2013; 136: 0110111–01101111.
14. Verstraete T and Li J. Multi-objective optimization of a U-bend for minimal pressure loss and maximal heat transfer performance in internal cooling channels. In: *ASME turbo expo 2013: Power for land, sea and air*, Texas, USA, 3 June–7 June 2013, paper no. GT2013-95423, pp.VO3AT12A041.
15. Lee KD, Kim SM and Kim KY. Multi-objective optimization of a row of film cooling holes using an evolutionary algorithm and surrogate modeling. *Numer Heat Transf A-Appl* 2013; 63: 623–641.
16. Nowak G and Wróblewski W. Cooling system optimisation of turbine guide vane. *Appl Therm Eng* 2009; 29: 567–572.
17. Chi Z, Liu H and Zang S. Geometrical optimization of nonuniform impingement cooling structure with variable-diameter jet holes. *Int J Heat Mass Transf* 2016; 136: 549–560.

18. El Ayoubi C, Ghaly W and Hassan I. Aerothermal shape optimization for a double row of discrete film cooling holes on the suction surface of a turbine vane. *Eng Optim* 2014; 47: 1384–1404.
19. Storn R and Price K. Differential evolution–a simple and efficient heuristic for global optimization over continuous spaces. *J Global Optim* 1997; 11: 341–359.
20. Kamble LV, Pangavhane DR and Singh TP. Neural network optimization by comparing the performances of the training functions -Prediction of heat transfer from horizontal tube immersed in gas–solid fluidized bed. *Int J Heat Mass Transf* 2015; 83: 337–344.
21. Li X and Wang T. Effects of various modeling schemes on mist film cooling simulation. *J Heat Transf* 2007; 129: 472–482.
22. Dávalos JO, García JC, Urquiza G, et al. Prediction of film cooling effectiveness on a gas turbine blade leading edge using ANN and CFD. *Int J Turbo Jet Eng*, Epub ahead of print 21 June 2016. DOI: 10.1515/tjj-2016-0034.

Appendix

Notation

A	area
b	ANN bias
c	semi-circular chord length
C	crossover rate parameter
D	diameter
f, g	hyperbolic tangent sigmoid functions, linear function
F	differential evolution scale factor
in	ANN inputs
l	profile length
$\dot{m}$	air mass flow
M	blowing ratio
n	number of cooling holes
O	ANN output
$\boldsymbol{p}, \boldsymbol{q}, \boldsymbol{r}$	differential evolution vectors
r	random number
T	temperature
v	velocity
$\boldsymbol{V}$	design vector
$w_\eta, w_{\dot{m}}$	importance weights
$\boldsymbol{X}, \boldsymbol{Y}, \boldsymbol{Z}$	differential evolution vectors
y^+	y plusFigures 2, 6, 7 and 10 are poor quality images, please provide the better quality figures.
η	cooling effectiveness
ρ	density
ω	ANN weights

Subscripts

aw	adiabatic wall
Aav	area averaged
c	coolant
in	input layer
k	number of neurons in input layer
l	number of neurons in output layer
m	mainstream
n	vector length
obj	objective
out	output layer
s	number of neurons in hidden layer
t	number of vector
tar	target

Superscripts

g	number of generation